16th World Conference on Earthquake, 16WCEE 2017

Santiago Chile, January 9th to 13th 2017

Paper N° 3532

Registration Code: S-J1464325820

Numerical and Experimental Evaluation of a Model Accuracy Indicator for Hybrid Simulations Involving Model Updating

S. Richardson[1], C. Chen[2] and N. Avramova[3]

[1] *Graduate student, School of Engineering, San Francisco State University, San Francisco, CA 94132, srr@mail.sfsu.edu*
[2] *Associate Professor, School of Engineering, San Francisco State University, San Francisco, CA 94132, chcsfsu@sfsu.edu*
[3] *Engineer, City of Mountain View, 500 Castro St, Mountain View, CA 94041, Neli.Avramova@mountainview.gov*

Abstract

Laboratory experiments play a critical role in earthquake engineering research. Hybrid simulation provides a viable technique to assess structural performance through component tests. One challenge exists for current practice of hybrid simulation when a complex structure has more critical components than those could be accommodated in laboratories. Hybrid simulation with model updating has been developed to updating the model parameters for analytical substructures based on the observed behavior of similar parts within experimental substructures. Hybrid simulation with model updating thus has great potential to be extended to real-time hybrid simulation to account for rate-dependent behavior within structures beyond existing laboratory capacity in terms of space and equipment. It however also raises concern on how to quantify the cumulative effect of modeling errors in analytical substructures throughout the experiments. This paper evaluates a previously developed tool using experimental results. The proposed tool is demonstrated to be highly effective for assessing the effect of modeling error and thereby enables future reliability assessment of hybrid simulation results when actual structural response is not available for immediate comparison.

Keywords: hybrid simulation, model updating, reliability, Kalman Filter

1. Introduction

Laboratory experiments play an important role in earthquake engineering research for performance evaluation of civil engineering structures under earthquakes. Conventional experimental methods (e.g., quasi-static tests, quasi-static pseudo-dynamic tests, and shaking table tests) are often constrained by limitations in laboratory space and testing equipment, and are thus not able to satisfy the needs of modern earthquake engineering research for large- or full-scale structural tests. As a result, conventional structural experiments are typically conducted only for the most critical parts of a structure at the component level and on a reduced scale. Such experiments pose serious problems for extrapolating the behavior of a particular component to the behavior of not only the entire system but also from a reduced scale to the full scale. The hybrid simulation technique [1-7], also known as the substructure technique, provides a viable solution to overcome space and equipment constraints and enable researchers to assess entire structural performance through component tests. Not well understood key components of the structure are physically tested as experimental substructures in laboratories, while well-behaved parts are numerically simulated as analytical substructures in computer programs. A numerical integration algorithm is utilized to integrate all different substructures to solve for the structural response under earthquakes.

A key challenge exists for current practice of hybrid simulation when a complex structure has more critical components than that laboratories can accommodate. More recently, the hybrid simulation technique was integrated with model updating [8-10]. Similar critical parts exist in both experimental and analytical substructures. Throughout the experiment, measured responses from the experimental substructures are used to refine the numerical models for critical parts within analytical substructures to improve their prediction for the rest of the test. This has been achieved successfully with the Unscented Kalman Filter (UKF) [11-13] and more recently with the Constrained Unscented Kalman Filter (CUKF) [14]. Thus, hybrid simulation only requires the physical representation of a smaller percentage of critical parts within the complex structure to derive the entire structural response. Fact-finding experiments using hybrid simulation with model updating were conducted for simple structures [8-10]. These exploratory researches also demonstrated that modeling errors in analytical substructures could have detrimental effects on the accuracy of entire hybrid simulation results. The inevitable modeling error due to estimation of the numerical parameters will lead to undesired inaccurate structural responses, including incorrect restoring forces of the analytical substructures. These errors will then propagate and accumulate during the entire experiment. It is necessary to quantify the cumulative effects of modeling error on the accuracy of the hybrid simulation to replicate the structural response under earthquakes. It is therefore critical to quantify the effect of the inaccurately estimated parameters for hybrid simulation with model updating to enable it to be used more properly and reliably for the earthquake engineering community.

2. Model Accuracy Indicator

A model accuracy indicator (*MAI*) was proposed by Chen *et al.* [15] to quantify the cumulative effect of modeling errors that can occur during hybrid simulation of complex structures. The definition of *MAI* is based on the synchronized subspace plot, as shown in Figure 1, between the restoring forces of the experimental and analytical substructure subjected to the same displacement history. The definition of MAI can be described as

$$MAI_{i+1} = 0.5(A_{i+1} - TA_{i+1}) \tag{1}$$

where i represents the current time step; A_{i+1} and TA_{i+1} are the enclosed and complementary enclosed areas for the i+1th time step; and MAI_{i+1} is the model accuracy indicator for the i+1th time step.

$$A_{i+1} = A_i + 0.5(F_{i+1}^{exp} + F_i^{exp}) \cdot (F_{i+1}^{ana} - F_i^{ana}) \tag{2a}$$

$$TA_{i+1} = TA_i + 0.5(F_{i+1}^{ana} + F_i^{ana}) \cdot (F_{i+1}^{exp} - F_i^{exp}) \tag{2b}$$

where F^{exp} and F^{ana} are the restoring forces of the experimental and analytical substructures, respectively. An accurate model for the critical part in the numerical substructure will lead to exactly same restoring force as that of experimental substructure measured during the experiment. In this case, the enclosed area of the synchronized subspace is equal to zero.

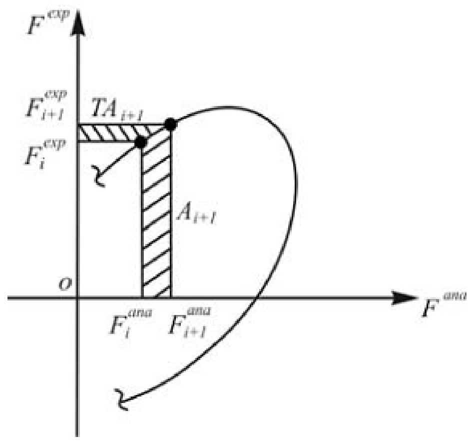

Figure 1. Schematic Synchronized Subspace Plot of MAI

3. Kalman Filter

Kalman filter is an estimator for problems which require knowledge of the instantaneous system state [16]. It has been useful in applications for complex dynamic systems where it may not be possible to measure all variables of interest. The unscented Kalman filter is often used for nonlinear systems with the discrete state space and measurement equations defined as:

$$x_{i+1} = f\,(x_i\,,\, u_i) \tag{3a}$$

$$y_{i+1} = h\,(x_{i+1},\, u_{i+1}) \tag{3b}$$

where x is the system state vector and u is the known input. The functions f and h represent the state and measurement functions, respectively. Typical application of Kalman filter involves first performing an unscented transform of the state space equation. The results are then fed to the measurement equation and another unscented transform will be performed. Then the Kalman filter gain will be calculated and applied to a comparison between the estimated mean of the measurement equation and an actual measurement of the real system. From this a new estimation of the state space will be derived for "updating" the system.

Wang and Wu [14] analyzed the effect of model updating through the Constrained Unscented Kalman Filter (CUKF). The typical Kalman filter can randomly pick its sigma points which can cause problems since specific values may cause instability of the system. To avoid this instability issue, the prediction step involving the state space equation and the correction step involving the measurement equation are conducted separately. For the prediction steps the points violating the constraints will be projected back on to the bounds. Furthermore, the symmetrical points will be scaled back similarly to maintain this symmetry. For the correction step violating sigma points will be pulled back to the boundary without regards for symmetry. For the CUKF an initial estimate of the system state "$\hat{x}_k$" is constructed from which the first set of sigma points "X_k" are selected

$$X_{k|k,\,i} = \hat{x}_{k|k}, \quad i = 0 \tag{4a}$$

$$X_{k|k,\,i} = \hat{x}_{k|k} + \theta_{k,i} s_{k|i}, \quad i = 1, 2, \ldots, 2n \tag{4b}$$

where $s_{k,i}$ is defined as the Cholesky factorization of the covariance matrix or

$$s_{k,i} = \left(\sqrt{P_{k|k}}\right)_i, \; i = 1,2,\ldots, n \tag{5a}$$

$$s_{k,i} = -\left(\sqrt{P_{k|k}}\right)_{i-n}, \ i = n+1, n+2, \ldots, 2n \tag{5b}$$

and θ_k is the sampling step size

$$\theta_{k,i} = \sqrt{(n+\kappa)}, \ i = 1, 2, \ldots, 2n \tag{5c}$$

As discussed earlier initial constraints on the sigma points are set and if violated, the sampling step size will be adjusted to track the sigma points back to the defined boundaries. These methods are discussed in more depth in Wang and Wu [14]. This constrained set of sigma points will then be subjected to the state space function to generate a preliminary set of sigma points for the next time step "$\mathbf{X}_{k+1|k}$" and its respective system state estimate $\hat{\mathbf{x}}_{\mathbf{k+1|k}}$.

$$X_{k+1|k,\ i} = f\left(X^{C}_{k|k,\ i}\right), \ i = 0,1,\ldots,2n \tag{6a}$$

$$\hat{x}_{k+1|k} = \sum_{i=0}^{2n} W_{k,i} X_{k+1|k,\ i} \tag{6b}$$

The preliminary system state estimate will be used for the measurement equation to generate measurement sigma points "$\mathbf{Y}_{k+1}$" and a measurement estimate "$\hat{\mathbf{y}}_{k+1}$"

$$Y_{k+1|k,\ i} = h\left(X_{k+1|k,\ i}\right), \ i = 0, 1,\ldots,2n \tag{7a}$$

$$\hat{y}_{k+1|k} = \sum_{i=0}^{2n} W_{k,i} Y_{k+1|k,\ i} \tag{7b}$$

Then a measurement covariance matrix "$\mathbf{P}_{yy}$" and the cross covariance matrix "$\mathbf{P}_{xy}$" are generated which is used to derive the Kalman filter gain "$\mathbf{K}_{k+1}$"

$$P_{yy,k+1|k} = \sum_{i=0}^{2n} W_{k,i}\left(Y_{k+1|k,\ i} - \hat{y}_{k|k}\right)\left(Y_{k+1|k,\ i} - \hat{y}_{k|k}\right)^{T} + R_{k+1} \tag{8a}$$

$$P_{yy,k+1|k} \sum_{i=0}^{2n} W_{k,i}\left(X_{k+1|k,\ i} - \hat{x}_{k|k}\right)\left(Y_{k+1|k,\ i} - \hat{y}_{k|k}\right)^{T} \tag{8b}$$

$$K_{k+1} = P_{xy,k+1|k} P^{-1}_{yy,k+1|k} \tag{8c}$$

The Kalman filter gain is then used to calculate the updated sigma points "$\mathbf{X}_{\mathbf{k+1|k+1}}$" for the next time step using a comparison between the measurement sigma points and a measurement "$\mathbf{y}_{\mathbf{k|k}}$" from a live experiment

$$X_{k+1|k+1,\ i} = X_{k+1|k,\ i} + K_{k+1}\left(y_{k|k} - Y_{k+1|k,\ i}\right), \ \ i = 0, 1,\ldots, 2n \tag{9}$$

The next step system state estimates "$\hat{\mathbf{x}}_{\mathbf{k+1|k+1}}$" and covariance matrices "$\mathbf{P}_{\mathbf{k+1|k+1}}$" are then calculated using

$$\hat{x}_{k+1|k+1} = \sum_{i=0}^{2n} W_{k,i} X_{k+1|k+1,\ i} \tag{10a}$$

$$P_{k+1|k+1} = \sum_{i=0}^{2n} W_{k,i}\left(X_{k+1|k|1,\ i} - \hat{x}_{k+1|k+1}\right)\left(X_{k+1|k+1,\ i} - \hat{x}_{k+1|k+1}\right)^{T} + Q_k + K_{k+1} R_{k+1} K^{T}_{k+1} \tag{10b}$$

and a final analysis is done to project any estimates that violate the constraints back to their bounds where $\mathbf{Q}_{\mathbf{k}}$ is the process noise covariance matrix and R_{k+1} is the observation noise.

4 Bouc-Wen Model

The Bouc-Wen model is used in this study to emulate the responses of the experimental and numerical substructures. The equation of motion for a single degree of freedom structure can be expressed as following

$$m \cdot \ddot{x}(t) \ + \ c \cdot \dot{x}(t) \ + r(t) = F(t) \tag{11}$$

where m is the mass; c is the inherent viscous damping; $r(t)$ is the restoring force; $F(t)$ is the earthquake excitation force; and $\dot{x}(t)$ and $\ddot{x}(t)$ are the velocity and acceleration responses, respectively. For hybrid simulation the restoring force of the SDOF structure is assumed to be composed of two parts:

$$r(t) = \mathrm{r^a(t)} + \mathrm{r^e(t)} \tag{12}$$

where $r^a(t)$ and $r^e(t)$ are the restoring forces of the analytical and experimental substructures, respectively. For the Bouc-Wen model the restoring force is defined by the nonlinear equation set of

$$r(t) = \alpha \cdot k \cdot x(t) + (1 - \alpha) \cdot k \cdot z(t) \tag{13a}$$

$$\dot{z}(t) = \dot{x}(t) - \gamma \cdot \dot{x}(t) \cdot z(t) \cdot |z(t)|^{n-1} - \beta \cdot \dot{x}(t) \cdot |z(t)|^{n} \tag{13b}$$

Description of the parameters is provided in Table 1 for the Bouc-Wen model used in this study.

Table 1 – Summary of Bouc-Wen Parameters for SDOF simulation

Parameter	**Description**
α	Ratio of elastic to inelastic stiffness
β	Basic hysteresis shape control
γ	Basic hysteresis shape control
k	Initial elastic stiffness
n	Sharpness of yield

5. Computational Simulation

Computational simulation is first conducted to evaluate the effectiveness of the MAI to track the effect of inaccurately estimated model parameters in the analytical substructures. Both single-degree-of-freedom and two-degree-of-freedom structures are considered for the computational simulation. For the constrained unscented Kalman filer, the state space equation is set as $f(\mathrm{x}) = \mathrm{z}(\mathrm{t}, \mathrm{v}, \gamma, \beta, n)$ and the measurement equation is set as $h(\mathrm{f(x)}) = r(t, k, \alpha, x(t), z(t))$. The system state vector is defined as $\mathbf{x} = [z, k, \beta, \gamma, n, \alpha]^{\mathbf{T}}$ initially in analytical substructures a system state estimate $\hat{\mathbf{x}} = [x_1, x_2, x_3, x_4, x_5, x_6]^{\mathbf{T}}$ is selected which will be the initial estimated values of the system state. An initial covariance matrix $\mathbf{P_0}$ will also be selected based on the confidence of these estimations. Additionally there will observation noise R_{k+1} and a process noise covariance matrix $\mathbf{Q_k}$ which contributes to the rate at which a solution is found.

5.1 Single-Degree-of-Freedom (SDOF) Structure

The single-degree-of-freedom steel chevron buckling braced frame is schematically shown in Figure 2. The structure is divided into two categories of interest, the braces and the surrounding frame. One brace is physically tested while the other is numerically modeled with parameters updated throughout the test. The frame has a beam assumed to be infinitely stiff. The braces are assumed to carry all the lateral stiffness amongst the vertical elements. It can be observed that the experimental and analytical substructures are subjected to the same displacement response during the hybrid simulation.

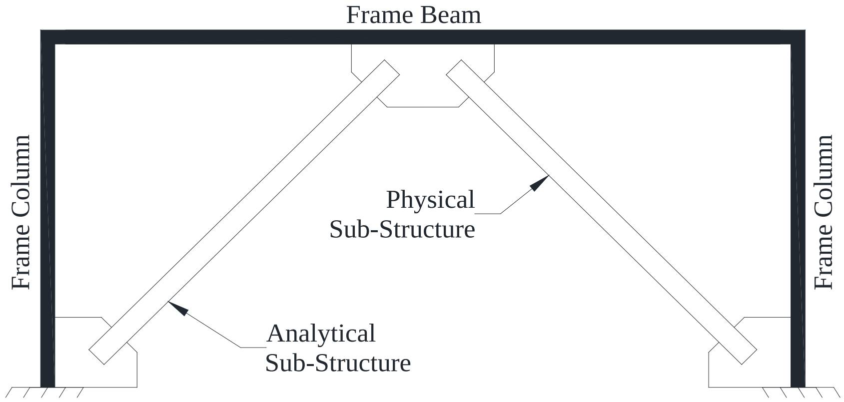

Figure 2. Schematic of Single-Degree-of-Freedom Steel Chevron Buckling Braced Frame

The parameters of the Bouc-Wen model for the experimental substructure are selected as k = 135 kN/mm, β = 0.55, γ = 0.45, n = 2, and α = 0.02; while the parameters for the numerical substructure are intentionally selected with error as k = 100 kN/mm, β = 0.2, γ = 0.2, n = 3, and α = 0.05. The bounding properties of the *CUKF* are $k \geq 0$, $\beta \geq 0$, $n \geq 1$, and $0 \leq \alpha \leq 1$. The Kalman filter has the properties $\mathbf{Q_k} = 10^{-6}\,\mathbf{I_6}$, R_{k+1} = 1.5 kN^2, and $\mathbf{P_0} = \mathrm{diag}(10^{-6}, 100, 10, 10, 10, 10^{-2})$. The process noise covariance matrix and the observation noise were tuned to represent the actual noise during the experiments. The initial covariance matrix is based on the confidence of the initial estimates. Since z is a calculated value a small corresponding index coefficient of 10^{-6} is used. For the purpose of simulation it is assumed that stiffness value was not well known and therefore given the highest corresponding indices of 100. However for most practical applications the initial stiffness will be readily available from static tests. The simulation is initially conducted for the 1994 Canoga park ground motion scaled with peak ground acceleration (PGA) of 1000 mm/sec. It is then repeated for the same ground motion scaled by different factors of 1.5, 2, 2.5 and 3.0 to evaluate the effectiveness of the MAI when the substructures develop nonlinear behavior. All the simulations are then compared to the corresponding simulation with exact parameter values for both analytical and experimental substructures. The root-mean-square (RMS) errors are calculated and presented in Table 2.

Table 2 – RMS Error for Simulations using Different Ground Motion Scales

Scale	**1.0**	**1.5**	**2.0**	**2.5**	**3.0**
RMS (10^{-5})	3.76	4.95	3.49	1.80	0.12

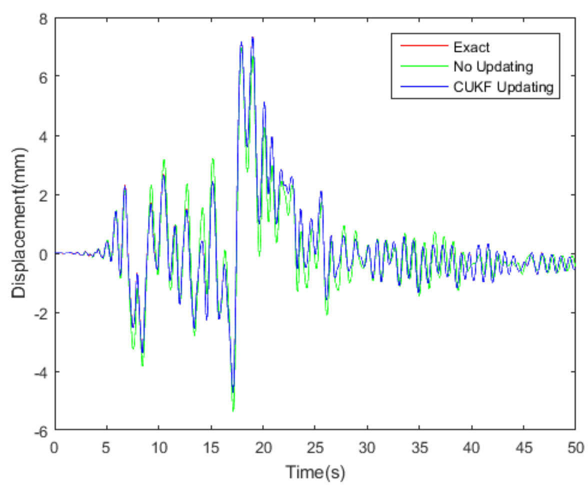

Figure 3. Comparison of Displacement Responses for Simulations of Exact, No Updating, and CUKF Updating for Ground Motion with PGA of 1000 mm/sec^2

The *RMS* values in Table 2 indicate little correlation between ground motion scale and accuracy of hybrid simulation with model updating. It also shows that the CUKF generates very accurate results as all errors are smaller than 1E-5. Figure 3 shows the time history of simulated displacement responses with and without updating in comparison with exact response. It can be observed that model updating using CUKF could help achieve accurate results. Figure 4a further demonstrates this through comparing the restoring forces.

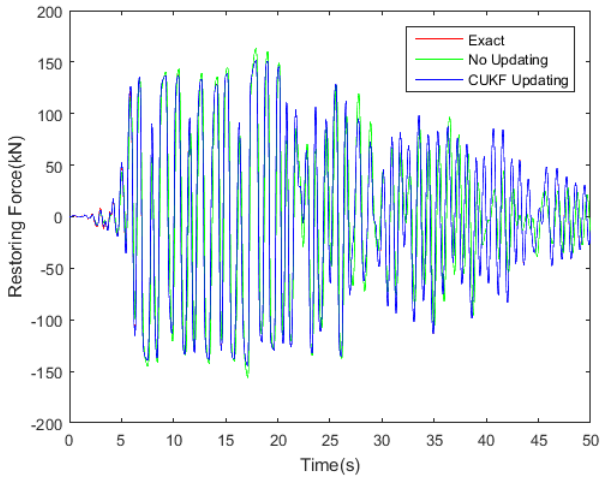

Figure 4a. Comparison of Restoring Forces for Simulations with Ground Motion PGA of 1000 mm/sec^2

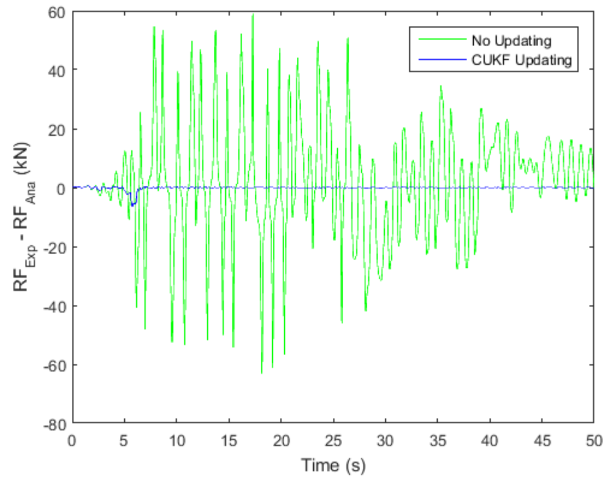

Figure 4b. Difference between Analytical and Physical Restoring Forces for Simulations with Ground Motion PGA of 1000 mm/sec^2

It can be observed in Figure 4a that difference initially exists between exact restoring force and the simulated restoring force with model updating. As time progresses the two restoring forces become almost the same. This is expected due to the nature of the *CUKF* which attempts to correct the numerical model to match the restoring force from the experimental substructure. This correction is observed by Figure 4b which shows the difference between analytical and physical restoring forces from an updated and non-updated case. It is clearly illustrated that the *CUKF* is effectively correcting the analytical substructure. The time histories of *MAI* are compared and presented in Figures 5 and 6 between simulations with and without model updating and at different ground motion scales.

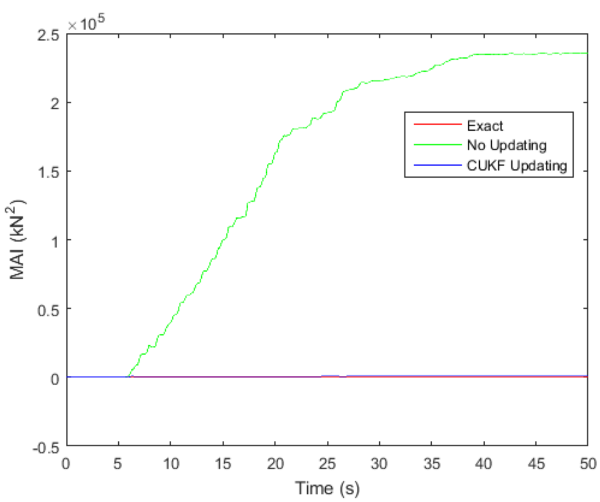

Figure 5. Time history of *MAI* for Simulations with and without Model Updating scaled to 1000 mm/sec^2

It can be observed in Figure 5 that the MAI successfully captures the effect of the error within the model parameters of the analytical substructures. The simulation without model updating has the largest values of MAI throughout the entire duration with maximum value around 2E05 kN^2. The model updating with CUKF demonstrably reduces the value of MAI thus minimizing the effect of modeling error in the analytical substructures. Figure 6 presents the time histories of MAI for simulations with model updating when the structure is subjected to different ground motion scales. It can be observed that, there does not exist an obvious correlation between ground motion scale and MAI. When the ground motion scale increases from 1.0 to 1.5, the maximum value of *MAI* increases; however the *MAI* decreases with ground motion scale increasing from 1.5 to 3.0. This implies that the *CUKF* was able to more reliably come to an accurate result as the input force increased, thus decreasing modeling error.

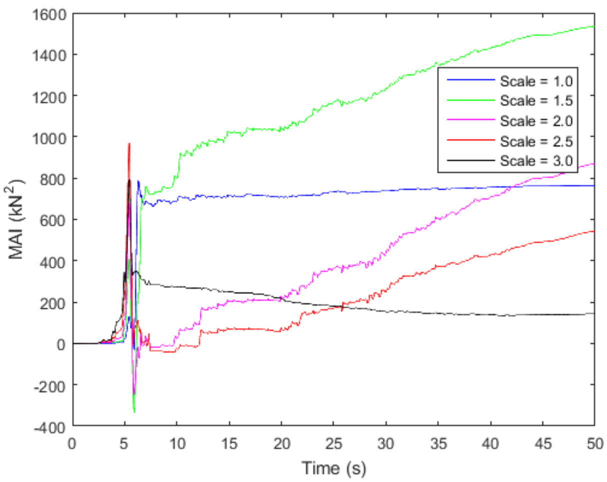

Figure 6. Time history of *MAI* for simulations with different scales of ground motion

5.2 Multiple-Degree-of-Freedom (MDOF) Structure

A two-story one-bay steel buckling restrained braced frame shown in Figure 7 is considered for evaluating the MAI for multiple-degree-of-freedom structures. The entire steel frame is analytically modeled except for the first story brace. The beams are assumed to have infinite stiffness and the columns are assumed to have $1/8^{th}$ of the stiffness of the braces. It can be observed that in this MDOF case, the experimental and analytical substructures will undergo different displacement responses.

Both braces are assumed to have properties consistent with the Bouc-wen Model by Black *et al*. [17]. The brace for experimental substructure is defined by the set properties of k = 414.5 kN/mm, β = 0.55, γ = 0.45, n = 1, and α = 0.025 while the brace for analytical substructure has estimated parameters of k = 415 kN/mm, β = 0.1, γ = 0.1, n = 3, and α = 0.04. The estimated parameters k and α is close to the actual values as the stiffness and post yield stiffness will likely be accurately obtained through mechanics or static load testing. The properties of the CUKF will be the same as the SDOF case except for the initial covariance matrix $\mathbf{P_0}$ = $\mathrm{diag}(10^{-6}, 10^{-8}, 100, 100,\ 100,\ 10^{-3})$. The covariance matrix is updated to reflect that the stiffness and post yield stiffness are more accurately known that the other parameters and therefore their corresponding covariance may be lower. Figure 8 presents the adaptation of the parameters for the simulation when the structure is subjected to the Canoga ground motion scaled to have PGA of 1000 mm/s^2.

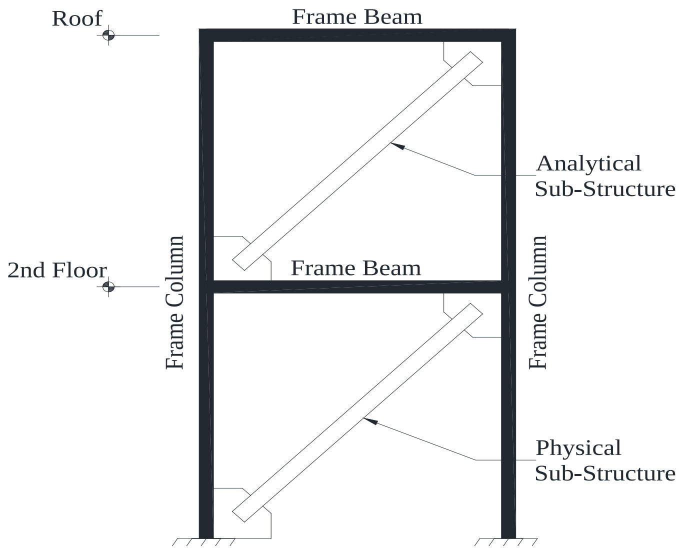

Figure 7. Two Degree of Freedom Frame Schematic

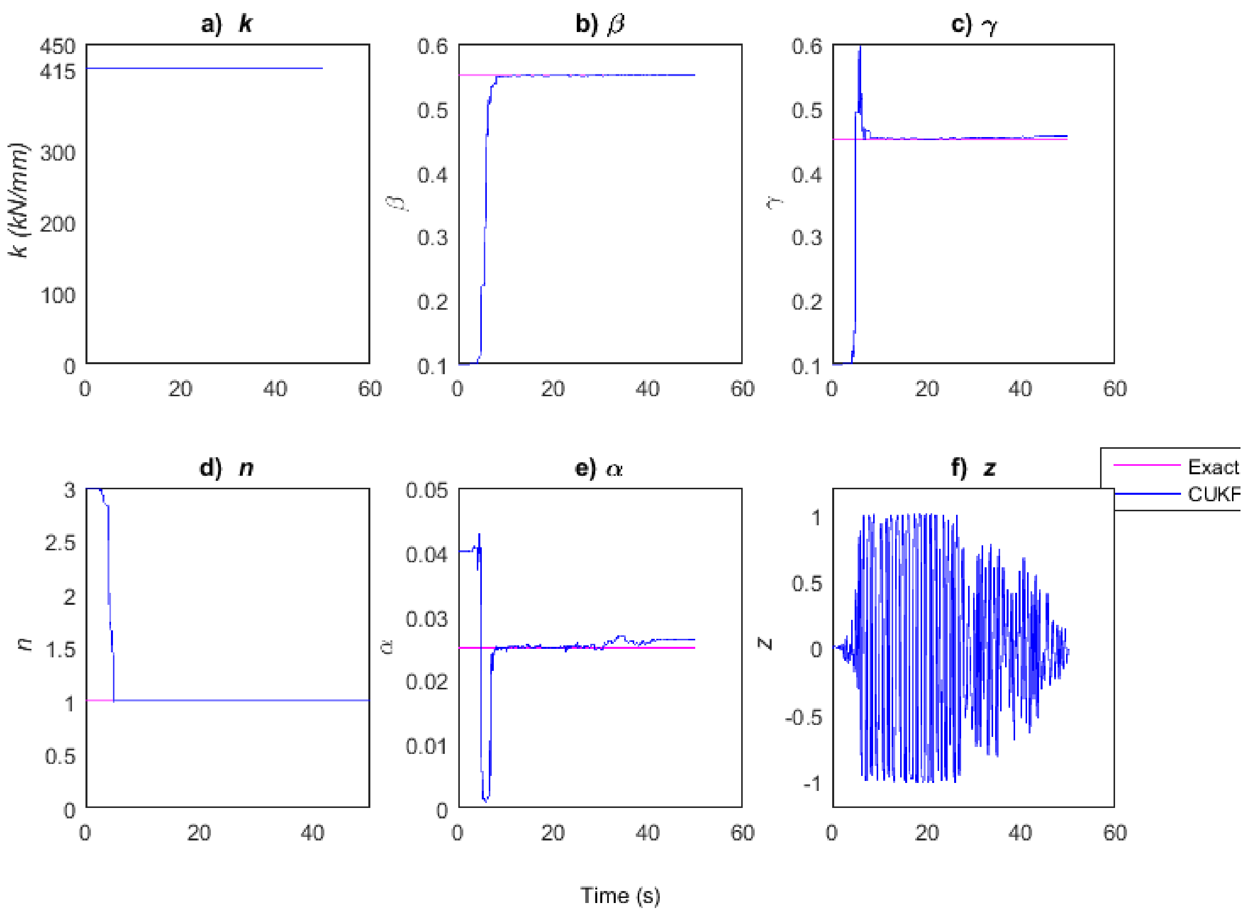

Figure 8. Time Histories of Parameters through CUKF: a) k, b) β, c) γ, d) n, e) α, and f) z

Figure 8 shows the updating of the Bouc-wen parameters in the analytical substructure over time. The parameters of the analytical model are observed to converge to the accurate values. The displacement responses of the 2nd and roof level of the structure are presented in Figure 9. Little difference can be observed between the displacements of two stories. Figure 10 shows that a majority of the yielding occurred in the brace framing into the 2nd floor for this simulation. This could have contributed to the difference in story drifts.

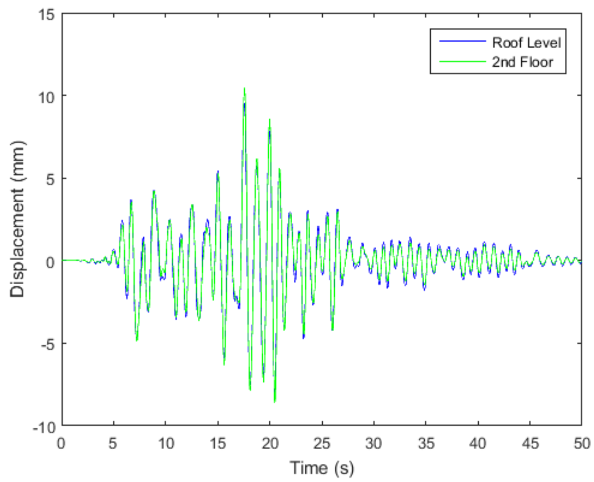

Figure 9. Displacement Responses of Roof and 2nd Floor

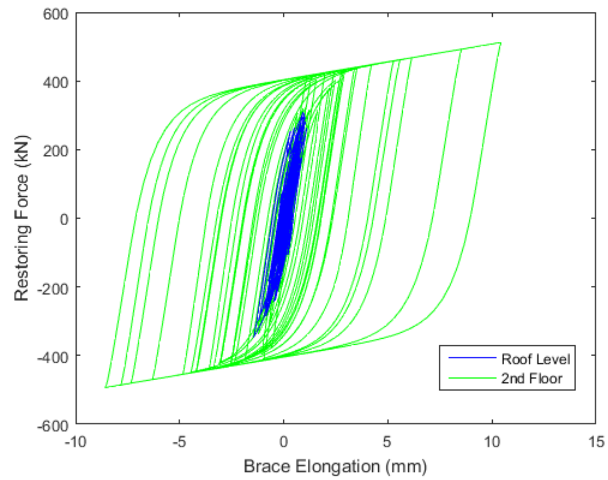

Figure 10. Hysteresis of Braces in Roof and 2nd Story

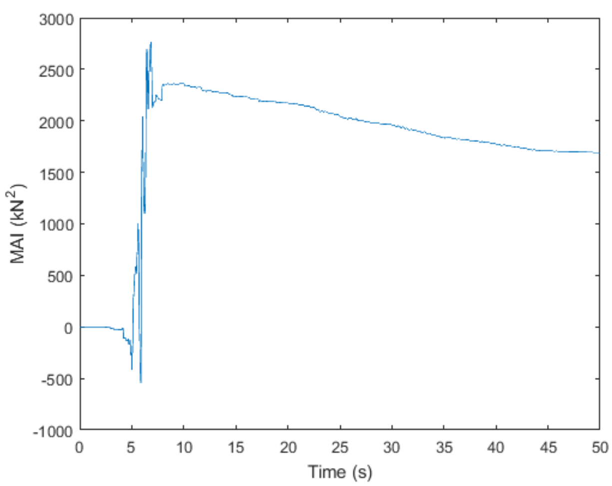

Figure 11. Time History of MAI

The time history of the MAI is presented in Figure 11. The MAI indicates that some of the accumulated error decreased after initially peaking. This could suggest that the online model updating could be over tuned causing potentially unrealistic results. When the constrained unscented Kalman filter perfectly updates the model, the MAI slope is expected to have the slope of 0. In the case where the MAI begins decreasing the Kalman filter could be shut off or toned down to keep the simulation stable.

5. Application of MAI to Experimental Results

The effectiveness of the MAI is further evaluated by the experimental results by Wang and Wu [15], which involves the real-time hybrid simulation of a SDOF two-bay braced frame with one brace numerically modeled and the other physically tested.

The synchronized subspace plot in Figure 12 indicates that there was error in the numerical modeling of the analytical substructure. The time history of the MAI in Figure 13 further confirm this with its value increasing monotonically from zero to the maximum value around 7E+5 kN^2.

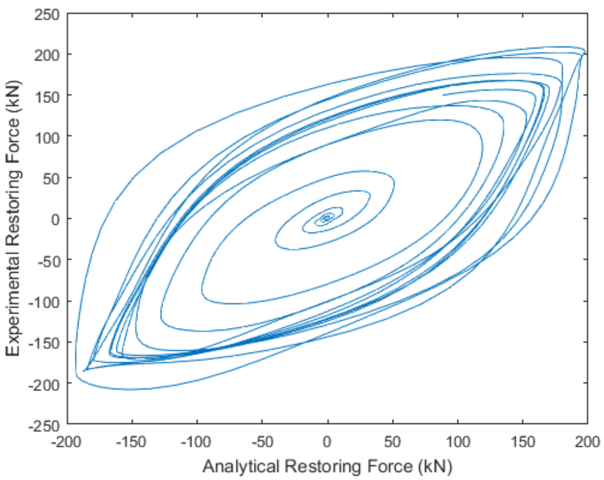

Figure 12. Subspace Plot of Experimental *RTHS* test

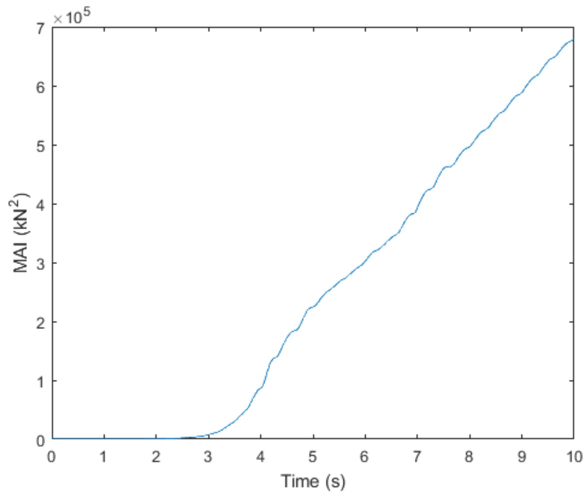

Figure 13. MAI Time History of Experimental Results

6. Summary, Conclusions, and Future Work

Online model updating makes it possible to extend the existing hybrid simulation technique to more complex civil engineering structures beyond the limits of laboratory space and servo-hydraulic equipment. Updating the numerical model of the analytical substructures based on the measurements from the experimental substructure presents a challenge to interpret the reliability of hybrid simulation results. This study presents numerical evaluation of a recently proposed MAI to quantify the cumulative effect of modeling error in hybrid simulation with model updating. The MAI is further demonstrated through experimental results. It is demonstrated that the MAI can effectively capture the cumulative effect of modeling error in analytical substructure thus providing a useful quantity for potential reliability assessment of hybrid simulation with model updating. However research still needs to be conducted to assess the accuracy of an updated hybrid simulation. The MAI aims to be a tool in the researcher's arsenal by showing cumulative system error through deviation in the analytical and experimental subspace plots.

However, this methodology has not been perfected. As seen in section 5.1 there is a significant reduction in the maximum MAI of the CUKF condition compared to the un-updated condition. Despite the reduction the MAI of the CUKF case indicates there is some modeling error. The MAI corresponding to an acceptable tolerance level of this error is currently unknown. In section 5.2 both braces where assumed to be the same so the experimental model could update the numerical model. Due to the simulated structures configuration larger forces occurred in the experimental substructure. Yielding occurred in this substructure however the force at the roof level was low enough to keep the analytical brace close to elastic. This does not line up with practical design considerations of distributing yielding evenly throughout a structure. Researchers doing online model updating should take this into consideration with a focus on finding ways to accurately update analytical substructures of different strength levels than their physical counterparts. Normalization of the MAI should also be explored to aid in interpretation of results. The MAI clearly can be used as a tool to observe the buildup of modeling error, however more work needs to be done to interpret the results.

7. Acknowledgements

This research was supported by the National Science Foundation under the award number CMMI-1227962. Any opinions, findings conclusions and recommendations expressed in this paper are those of the author and do not necessarily reflect those of the sponsors. The authors also appreciate the support from Professor Wu at Harbin Institute of Technology to share experimental results for this paper.

8. References

[1] Nakashima, M., Kato, H. and Takaoka, E. (1992). "Development of real-time pseudodynamic testing." Earthquake Engineering and Structural Dynamics, 21(1), 79-92.

[2] Horiuchi, T., Inoue, M., Konno, T. and Namita, Y. (1999). "Real-time hybrid experimental system with actuator delay compensation and its application to a piping system with energy absorber." Earthquake Engineering and Structural Dynamics, 28(10), 1121-1141.

[3] Horiuchi, T. and Konno, T. (2001). "A new method for compensating actuator delay in real-time hybrid experiment." Philosophical Transactions of the Royal Society of London A, 359, 1893-1909.

[4] Bonnet, P.A, Lim, C.N., Williams, M.S., Blakeborough, A., Neild, S.A., Stoten, D.P. and Taylor, C.A. (2007). "Real-time hybrid experiments with Newmark integration, MCSmd outer-loop control and multi-tasking strategies," Earthquake Engineering and Structural Dynamics, 36(1), 119-141.

[5] Jung, R.Y., Shing, P.B., Stauffer, E. and Thoen, Bradford. (2007). "Performance of a real-time pseudodynamic test system considering nonlinear structural response." Earthquake Engineering and Structural Dynamics, 36(12), 1785-1809.

[6] Christenson R., Lin, Y.Z., Emmons A. and Bass B. (2008). "Large-scale experimental verification of semi-active control through real-time hybrid simulation." Journal of Structural Engineering, 134(4), 522-534.

[7] Chen, C., Ricles, J.M., Marullo, T. and Mercan, O. (2009). "Real-time hybrid testing using the unconditionally stable explicit CR integration algorithm." Earthquake Engineering and Structural Dynamics, 38(1), 23-44.

[8] Zhang, J. (2010). An Adaptive Hybrid Simulation Testing Method. Master Thesis, Harbin Institute of Technology, Harbin, China (in Chinese).

[9] Mosqueda, G., Hashemi, M.J. and Masroor, A. (2012). "Hybrid Simulation with On-line Updating of Numerical Model Based on Measured Experimental Behavior." NEES Quake Summit, Boston, MA.

[10] Mosqueda, G. (2012). "Hybrid Simulation with On-line Updating of Numerical Model based on Measured Experimental Behavior." International Mini-workshop on Hybrid Simulation, May 18, Harbin Institute of Technology, Harbin, China.

[11] S. J. Julier and J. K. Uhlmann, "A general method for approximating nonlinear transformations of probability distributions," Technical Report, Robotics Research Group, Department of Engineering Science, University of Oxford, 1994.

[12] S. J. Julier and J. K. Uhlmann, "A new extension of the Kalman filter to nonlinear systems," Proceedings of AeroSense: The 11th International Symposium on Aerospace/Defense Sensing, Simulation and Controls, Multi Sensor Fusion, Tracking and Resource Management, SPIE, Orlando, FL, April 21–24, pp. 182–193, 1997.

[13] Wang T. and Wu B. (2012). "Model updating for hybrid testing with unscented Kalman filter", the 7th International Workshop on Advanced Smart Materials and Smart Structures Technology ANCRiSST2012, Bangalore, India, July, 27-28.

[14] Wang T. and Wu B. (2013), "Real-time Hybrid Testing with Constrained Unscented Kalman Filter," The 5th International Conference on Advances in Experimental Structural Engineering, NCREE, Taipei, Taiwan, November 8-9, 2013.

[15] Chen, C., Avramova, N., and Pong, W. (2013). "An Assessment Tool for Quantifying Cumulative Effect of Modeling Errors for Smart Hybrid Simulation." RASD 11th International Conference Pisa, Italy.

[16] Grewal, M. and Andrews, A. *Kalman Filtering*: *Theory and Practice using MATLAB. Third Edition*. Hoboken: John Wiley & Sons, 2008

[17] Black, C., Makris, N., and Aiken, I. (2004), "Component Testing, Seismic Evaluation and Characterization of Buckling-Restrained Braces. Journal of Structural Engineering, Vol. 130, No. 6, June 1, 2004.